

Strongly accelerated margination of active particles in blood flow

Stephan Gekle

Physikalisches Institut, Universität Bayreuth, Germany

Abstract

Synthetic nanoparticles and other stiff objects injected into a blood vessel filled with red blood cells are known to marginate towards the vessel walls. By means of hydrodynamic Lattice-Boltzmann simulations we show that active particles can strongly accelerate their margination by moving against the flow direction: particles located initially in the channel center migrate much faster to their final position near the wall than in the non-active case. We explain our findings by an enhanced rate of collisions between the stiff particles and the deformable red blood cells. Our results imply that a significantly faster margination can be achieved either technically by the application of an external magnetic field (if the particles are magnetic) or biologically by self-propulsion if the "particles" are, e.g., swimming bacteria.

1

One of the most prominent effects in blood flow is the margination, i.e., cross-streamline migration, of stiff particles towards the vessel walls (1, 2). This generic behavior is observed for naturally stiff objects such as platelets or leucocytes but also for synthetic nanoparticles which are used for drug-delivery or microdiagnosis applications. Margination is generally attributed to the hydrodynamic interaction of the soft red blood cells with the stiff particles as it has been found to disappear when red blood cells are removed from the liquid.

Margination has been observed experimentally as early as 1980 (3) and since then has been confirmed a number of times (4–9). Over recent years, computer simulations have been able to reproduce the effect using various techniques such as 2D Lattice-Boltzmann (8, 10–14), 2D dissipative-particle dynamics (15), 2D boundary-integral (16) as well as 3D boundary-integral methods (17–21), 3D dissipative-particle dynamics (22, 23), 3D lattice-Boltzmann (9, 24) and 3D immersed-boundary methods (25, 26). A number of quantitative mathematical models have been proposed in order to understand and to predict the margination effect (12, 20, 27–33). All these models have in common that they are based on the major role played by the interaction between the soft red blood cells and the stiff particles. While the steady margined state has been fairly well studied, rather little attention has been paid to the dynamics of margination. Investigations how long it actually takes for a stiff particle to marginate from the center of the channel to the vessel wall are rather scarce, with one recent notable exception (34).

Nevertheless, this question becomes relevant, e.g., when the margination effect is to be used for particle sorting applications where a homogeneously mixed suspension is flown from a large reservoir through a microfluidic channel and the goal is to extract the margined stiff particles at the end of the channel (35).

In this contribution we propose a simple mechanism which strongly accelerates the margination process by the application of an external force opposite (but not perpendicular) to the flow direction. The forcing can be achieved, e.g., by a magnetic field if the marginating particles are magnetic or by active swimming if the "particles" are living organisms such as bacteria. Using Lattice-Boltzmann simulations we demonstrate the effectiveness of our mechanism for spherical and elongated particles in cylindrical channels at various hematocrits as well as plane Poiseuille setups. Besides being of possible technical and biological relevance, our contribution underlines in an intuitive and pictorial way the importance of cell-particle collisions which occur much more frequently when the relative velocity between the particles and the RBCs is increased due to the external forcing.

Methods

We employ a combination of the three-dimensional Lattice-Boltzmann Method (LBM) with the Immersed Boundary Method (IBM). For our calculations we use the simulation program EsPREsSo (36–38) which we extended to include the IBM. The LBM solves the Navier-Stokes by discretizing space as well as velocities and is well described, e.g., in (39–41). The LBM implementation in EsPREsSo includes thermal fluctuations in the fluid (here we choose $T = 300\text{K}$).

¹Published as: Biophys. J. 110, 514-520 (2016), doi:10.1016/j.bpj.2015.12.005

The fluid properties are those typical of blood plasma with a viscosity $\eta = 1.2\text{mPas}$ and a density $\rho = 1000\text{kg/m}^3$.

The idea of the IBM is to model deformable particles by a discrete set of Lagrangian massless particles, whose positions are not restricted to the LBM lattice and which are advected with the (interpolated) flow velocity at each time step (42, 43). For the interpolation of the flow velocity at the off-lattice particle positions we use a simple eight-point stencil.

The RBC membrane is modelled as an infinitely thin elastic sheet endowed with a shear and area resistance according to the Skalak model (44–46). The shear modulus is $k_s = 5 \cdot 10^{-6}\text{N/m}$ (45) and the area dilation modulus is chosen as $k_a = 100k_s$. The bending resistance is modeled following the model of (47–49) with a bending modulus of $k_b = 2 \cdot 10^{-19}\text{Nm}$. To correct for numerical flux of mass through the membrane we employ an additional force to keep the RBC volume constant (49). The volume deviation of RBCs during the simulation is below 1%. To ensure numerical stability, a short-ranged soft-sphere repulsion is added between RBCs, stiff particles and the vessel walls.

The active particles are modelled by triangulated spheres whose interior space is filled with a regular three-dimensional grid of IBM nodes as illustrated in the Supporting Material. As usual in Immersed-Boundary-Methods the grid nodes are massless points flowing with the local fluid velocity. Thus, the interior of the active particles possesses the same density as the surrounding fluid. The grid nodes are connected by stiff harmonic springs as well as bending potentials to retain the rectangular grid arrangement. We found that choosing the grid constant for the stiff particles identical to the LBM grid distance (i.e. 1 in simulation units) yielded the best results. We note that modelling stiff particles in a naive way by using the RBC model described above endorsed with very stiff shear, dilatation and bending moduli, but without the interior grid, required unreasonably small time steps. Compared to IBMs which are explicitly intended for rigid particles (50) our method furthermore possesses the advantage that unphysical flows within the stiff particle are very efficiently suppressed by the interior grid. We monitored the deformation of the stiff particles during the simulation and found it to be negligibly small (see Supporting Information). The volume change of the stiff particle is on average below 2%. Our stiff particle model in addition satisfies very well the no-slip boundary condition on the particle surface as shown in the Supporting Information.

We have validated our method for red blood cells and stiff particles using literature data for the cell-free layer in various microchannels by (19, 51, 52) as detailed in the Supporting Information.

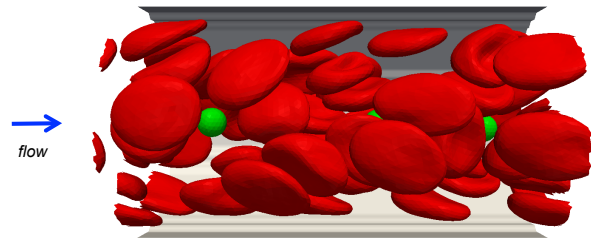


Figure 1: Snapshot of the investigated system: 52 red blood cells are mixed with 4 stiff particles (green) inside a $47\ \mu\text{m}$ long cylindrical channel with a radius $R = 13\ \mu\text{m}$. The stiff particles are initially located close to the channel center. The flow direction is from left to right and the external force on the stiff particles is applied from right to left thus slowing down the motion of the stiff particles. A corresponding movie can be found in the Supporting Material.

Results and Discussion

1.1 Accelerated margination

Figure 1 shows the initial setup of our simulation box. 52 red blood cells are placed randomly inside a cylindrical channel with radius $R = 13\ \mu\text{m}$ and length $47\ \mu\text{m}$ leading to a hematocrit of 18%. Four stiff spherical particles with radius $a = 1.6\ \mu\text{m}$ are added to the suspension such that their initial location is close to the center of the channel. A flow is applied from left to right whose pressure gradient is chosen such that the center velocity of a corresponding Poiseuille flow in the same channel without RBCs and particles would be $v_c = 2.5\text{mm/s}$. We then apply a force on the stiff particles directed opposite to the flow direction. Three strengths are considered: $F_1 = 6\pi\eta a v_c$ which exactly balances the Stokes friction, $F_2 = F_1/2$ and $F_3 = F_1/4$ which is shown in the Supporting Material.

Figure 2 shows the motion in flow direction of the stiff particles as a function of time. Since v_c represents an upper bound on the true velocity in the channel, F_1 is larger than the typical friction force and accordingly the particles exhibit a net motion contrary to the flow direction, while for F_2 the motion is in flow direction but significantly slower than in the force-free case.

Our main result is shown in fig. 3 where we compare the cross-streamline migration of the stiff particles towards the channel walls. As is to be expected, for all considered force strengths (including the force-free case) the stiff particles show a clear tendency to marginate towards the channel wall and to collect inside the cell-free layer. Once they reach the cell-free layer, the particles basically stay there apart from rather short excursions into the bulk flow. Yet, the time that is required by the particles to reach the cell-free layer starting from their initial position in the bulk flow is

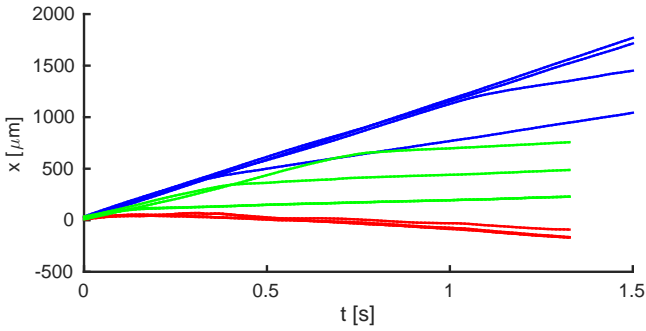


Figure 2: Motion of the four stiff particles in flow direction (each line corresponds to one particle). For strong counter-forces (F_1 , red lines) the net motion is against the flow direction, while for weak counter-forces (F_2 , green lines) the motion is in flow direction, but significantly slower than in the force-free case (blue lines).

strongly different in the three cases: if the strong counter-force F_1 is applied, the particles marginate much faster (within roughly 0.3s) than they do in the force-free case (2s). The margination speed with weak forcing F_2 (0.5s) is intermediate between F_1 and the force-free case. We note in passing that the distance travelled by the particles in the force-free case before complete margination² amounts to around 0.5cm in very good agreement with recent experiments and boundary-integral simulations (34).

It has been argued by a number of researchers that the principal cause of margination can be found in the heterogeneous collisions between stiff and deformable particles (12, 20, 30, 32, 33). It is intuitively clear that the counter-force applied in the present setup will lead to an increase in the number of collisions between the fast-moving RBCs and the slower stiff particles. We will now attempt to quantify the collision frequency for the different cases.

In a dense suspension such as the one considered here, a "collision" is somewhat difficult to define, however. As we observe extended periods during which a stiff particle and an RBC move side-by-side in close proximity (which should not be considered a collision) it is obvious that purely distance-based criteria will not be appropriate for the present system. We therefore revert to a dynamics-based criterion, namely the frequency of neighbor switches. For each stiff particle the RBC with the smallest surface-to-surface distance is considered as its neighbor. Every time that a stiff particle switches from one neighboring RBC to another, we consider that a collision has taken place. To avoid multiple countings due to small fluctuations, each neighbor change is counted only once. The result is shown in fig. 4. As can be seen, the frequency of collisions is increased if the particles are actively moving against the flow. Our results thus provide

²The distance can be estimated by considering the average margination time $t_m \approx 2s$ from the blue curves in fig. 3 and multiplying by the flow speed v_c .

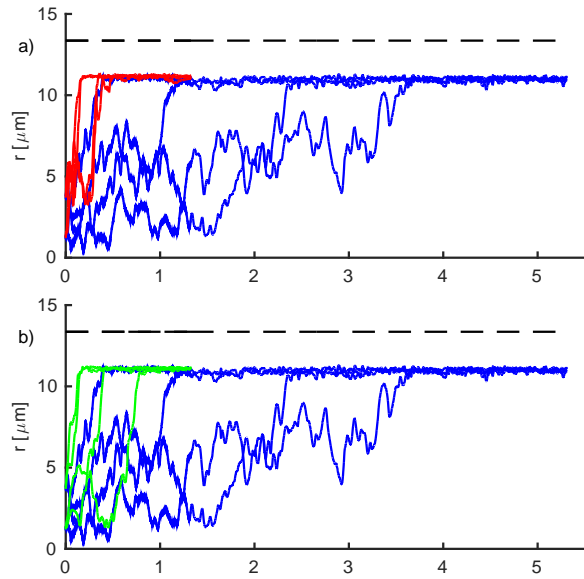


Figure 3: Margination dynamics of the four stiff particles. In the force-free case (blue lines in (a) and (b)) a clear tendency of the particles to migrate towards the cell-free layer near the channel wall (dashed line) is seen. The time until the cell-free layer is reached, however, can be significantly reduced by applying an external force directed opposite to the flow, both for strong (F_1 , red line in (a)) as well as intermediate forces (F_2 , green line in (b)).

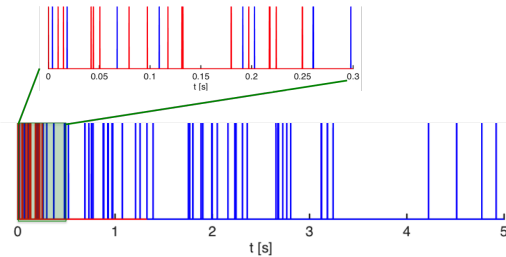


Figure 4: The frequency of collisions, as defined in the main text, between stiff particles and RBCs. The case with forcing (red) clearly shows an increased collision frequency as compared to the force-free case (blue). Once the stiff particles are completely margined, the collisions (almost) disappear.

evidence that increasing the number of collisions directly leads to an increase in the margination speed and thus serve to strengthen recent models which explain margination based on heterogeneous collisions (12, 20, 30, 32, 33).

1.2 Influence of hematocrit and particle shape

We now turn to investigate the influence of a changing hematocrit on the margination dynamics. Figure 5 (a) and (b) show the trajectories of the active stiff particles in figure 3 but with a hematocrit level of 11% and 32%. The setup with

11% hematocrit has been obtained by reducing the amount of RBCs from 54 to 32 with respect to the setup in figure 3 while the 32% case contains 54 RBCs in a shorter ($32\mu\text{m}$ instead of $47\mu\text{m}$) and slightly thinner ($R = 12.7\mu\text{m}$) channel with only two stiff particles. Clearly, the acceleration due to an external field is robust against changes in the hematocrit level. As a side note, we observe that the margination dynamics even in the field-free case (blue lines in Figs. 3 and 5) slows down at the high hematocrit.

Artificial nanoparticles or bacteria can have various shapes. To investigate how a deviation from the small sphere geometry affects the margination dynamics, we show in figure 5 (c) and (d) the trajectories for large spheres with radius $a = 3.2\mu\text{m}$ as well as elongated particles with an aspect ratio 2:1 as shown in the inset. We find no significant influence of this shape change on the margination dynamics.

1.3 Influence of system geometry

To ensure that our results are not restricted to the specific channel shown above, we investigate two further geometries. The first one is a thicker channel with radius $R = 21.8\mu\text{m}$ and length $L = 59\mu\text{m}$ containing 180 RBCs and 10 stiff particles. Figure 6 (a) compares the margination dynamics of the force-free case with the situation when the strong counter-force F_1 is applied.

The second system is a plane-Poiseuille setup consisting of two plane walls with a distance of $27\mu\text{m}$. The box (which is now periodic in the two lateral directions) has dimensions $23 \times 27\mu\text{m}$ in x - and y -direction, respectively. It is filled with 32 RBCs and 4 stiff particles and we choose a somewhat lower center velocity of $v_c = 0.6\text{mm/s}$ and a slightly different viscosity of $\eta = 1.02\text{mPas}$. The corresponding migration dynamics is shown in fig. 6 (b). The strongly accelerated margination dynamics observed for both systems in figure 6 confirms the general nature of our proposed mechanism.

1.4 Particle dynamics in the margined state

Finally, we comment on the particle dynamics in the margined state. From inspection of figures 3 to 6 a few trends are visible. As is to be expected, we note from figure 5 (a) that the margined state is in general less stable for the low hematocrit $Ht = 11\%$ than it is for the higher hematocrits. Comparing the situations with and without external driving, only for $Ht = 11\%$ a significant influence of the external driving can be discerned leading to short dips of the stiff particles into the main flow in figure 5 (a). These are caused by the combination of a low Ht together with a large relative velocity between the stiff particles and the RBCs. A further observation can be made in figure 5 (c) for the large particle. Here, the margined state is clearly much more stable than for the smaller spheres in agreement with

the margination mechanism proposed recently by Fedosov *et al.* (15).

Next, we investigate the rotation of the stiff particles in the margined state. As shown in figure 7 (a) the rotation around the x -axis (plain lines) is much smaller than the averaged rotation around the y and z axes (lines with asterisk). This is to be expected considering that the flow is in x direction. Here we also discern an influence of the external driving: with increasing force strength the rotation diminishes. Active particles exhibit a more sliding motion while non-active particles rather tend to roll along the channel walls.

The strongest influence of the external forcing is observed for the elongated particles in figure 5 (d). Here, the margined state of the active stiff particles is clearly less stable than the force-free case. To investigate the cause of this difference, we show in figure 7 (b) the rotation around the long and short axes of the elongated particle for the three cases F_1 , F_2 and without force. For the force-free case the particle rotates almost exclusively around the long axis, as is to be expected. With external driving, however, the particle exhibits a tumbling motion rotating around all three axes simultaneously. This different rotation explains the more noisy behavior of the red and green center-of-mass trajectories in figure 5 (d).

Conclusion

We have demonstrated a possibility for strongly accelerated margination dynamics of active particles in the blood stream: if particles move against the local flow direction, driven either by an external magnetic field or by self-propulsion, the relative velocity between the soft red blood cells and the active particles increases which in turn leads to an enhanced collision rate between the two. This enhanced collision rate triggers the accelerated migration of the active particles towards the cell-free layer near the channel walls. Our contribution thus furnishes a straightforward and intuitive illustration that indeed RBC-particle collisions are the main driving mechanism behind margination which is the central assumption used in recent mathematical models for the margination effect. The proposed mechanism might be of technical and biological relevance as it provides a simple method to efficiently isolate synthetic particles from a flowing blood stream and might represent a way for bacteria to travel towards the vessel walls simply by swimming against the local flow direction.

Acknowledgements

The author thanks the Volkswagen Foundation for financial support and acknowledges the Gauss Centre for Supercomputing e.V. for providing computing time on the GCS Supercomputer SuperMUC at Leibniz Supercomputing Centre.

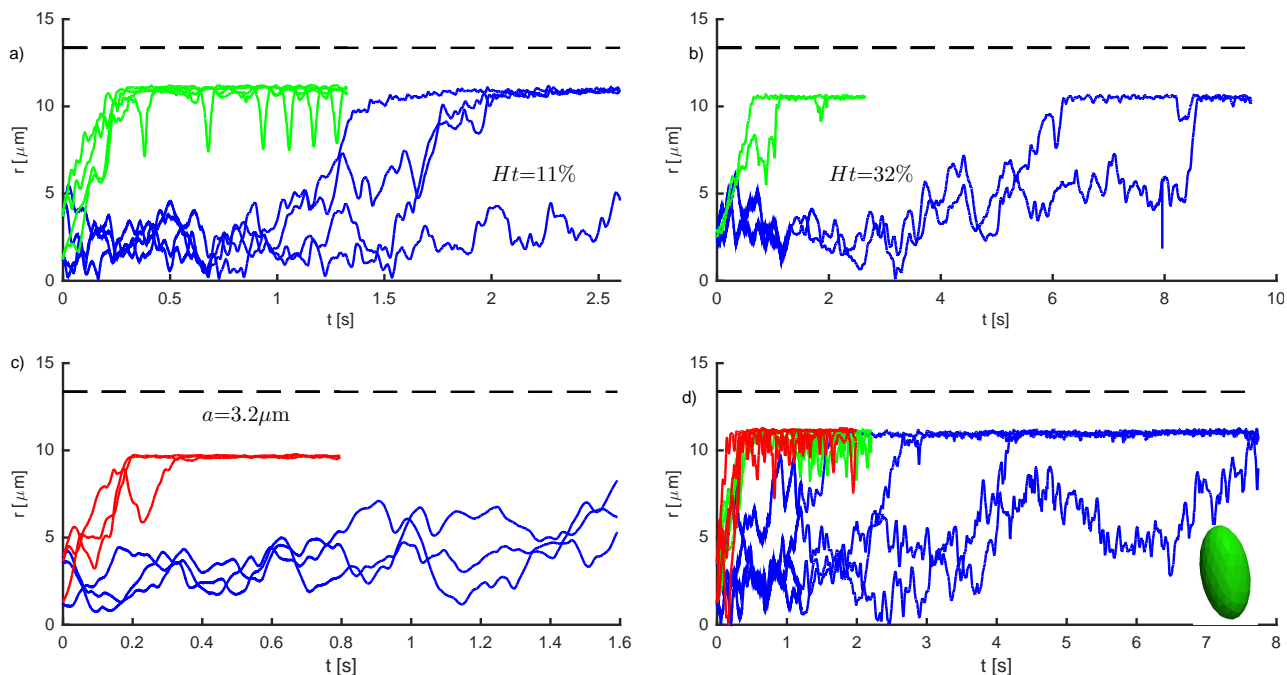


Figure 5: (a)+(b): margination dynamics at different hematocrits. For the field-free case (blue lines) we find that the time required to reach the margined state increases at the high hematocrit of 32%. The active particles with forcing F_2 (green) marginate significantly faster than the non-active particles. (c)+(d): The accelerating effect of the external forcing also appears for large spherical particles with forcing F_1 (c) as well as elongated ones with forcing F_1 (red) and F_2 (green) as shown in (d).

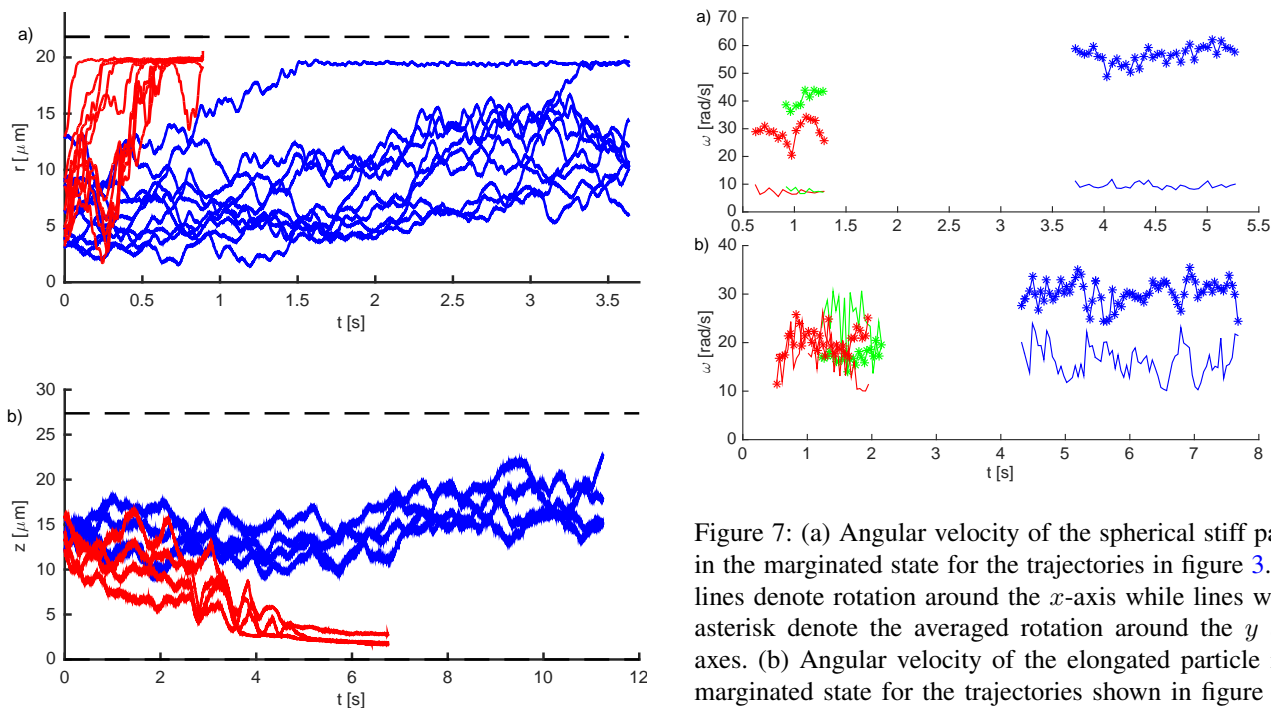


Figure 6: The accelerating effect of the external forcing F_1 (red lines) is confirmed also for different channel geometries: (a) a thick channel and (b) a plane Poiseuille setup.

Figure 7: (a) Angular velocity of the spherical stiff particle in the margined state for the trajectories in figure 3. Plain lines denote rotation around the x -axis while lines with an asterisk denote the averaged rotation around the y and z axes. (b) Angular velocity of the elongated particle in the margined state for the trajectories shown in figure 5 (d). Here, curves with an asterisk show rotation around the long axis in a body-fixed coordinate system while plain curves show the averaged rotation around the two short axes.

References

1. Popel, A. S., and P. C. Johnson, 2005. Microcirculation and hemorrheology. *Annu. Rev. Fluid Mech.* 37:43–69.
2. Misbah, C., and C. Wagner, 2013. *Comptes Rendus Physique. C. R. Physique* 14:447–450.
3. Schmid-Schönbein, G. W., U. Shunichi, R. Skalak, and S. Chien, 1980. The interaction of leucocytes and erythrocytes in capillary and postcapillary vessels. *Microvasc. Res.* 19:45–70.
4. Eckstein, E. C., A. W. Tilles, and F. J. I. Millero, 1988. Conditions for the occurrence of large near-wall excesses of small particles during blood flow. *Microvasc. Res.* 36:31–39.
5. Zhao, R., J. N. Marhefka, F. Shu, S. J. Hund, M. V. Kameneva, and J. F. Antaki, 2008. Micro-Flow Visualization of Red Blood Cell-Enhanced Platelet Concentration at Sudden Expansion. *Ann. Biomed. Eng.* 36:1130–1141.
6. Jain, A., and L. L. Munn, 2009. Determinants of Leukocyte Margination in Rectangular Microchannels. *PLoS ONE* 4:e7104.
7. Charoenphol, P., R. B. Huang, and O. Eniola-Adefeso, 2010. Potential role of size and hemodynamics in the efficacy of vascular-targeted spherical drug carriers. *Biomaterials* 31:1392–1402.
8. Lee, T.-R., M. Choi, A. M. Kopacz, S.-H. Yun, W. K. Liu, and P. Decuzzi, 2013. On the near-wall accumulation of injectable particles in the microcirculation: smaller is not better. *Sci. Rep.* 3:1–8.
9. Chen, H., J. I. Angerer, M. Napoleone, A. J. Reininger, S. W. Schneider, A. Wixforth, M. F. Schneider, and A. Alexander-Katz, 2013. Hematocrit and flow rate regulate the adhesion of platelets to von Willebrand factor. *Biomicrofluidics* 7:064113–12.
10. Migliorini, C., Y. Qian, H. Chen, E. B. Brown, R. K. Jain, and L. L. Munn, 2002. Red Blood Cells Augment Leukocyte Rolling in a Virtual Blood Vessel. *Biophys J* 83:1834–1841.
11. Ouared, R., B. Chopard, B. Stahl, D. A. Rüfenacht, H. Yilmaz, and G. Courbebaisse, 2008. Thrombosis modeling in intracranial aneurysms: a lattice Boltzmann numerical algorithm. *Comput. Phys. Commun.* 179:128–131.
12. Crowl, L. M., and A. L. Fogelson, 2011. Analysis of mechanisms for platelet near-wall excess under arterial blood flow conditions. *J Fluid Mech* 676:348–375.
13. Mountrakis, L., E. Lorenz, and A. G. Hoekstra, 2013. Where do the platelets go? A simulation study of fully resolved blood flow through aneurysmal vessels. *Interface Focus* 3:20120089–20120089.
14. Skorzewski, T., L. C. Erickson, and A. L. Fogelson, 2013. Platelet Motion near a Vessel Wall or Thrombus Surface in Two-Dimensional Whole Blood Simulations. *Biophys J* 104:1764–1772.
15. Fedosov, D., J. Fornleitner, and G. Gompper, 2012. Margination of White Blood Cells in Microcapillary Flow. *Phys. Rev. Lett.* 108:028104.
16. Freund, J. B., 2007. Leukocyte margination in a model microvessel. *Phys. Fluids* 19:023301.
17. Kumar, A., and M. Graham, 2011. Segregation by membrane rigidity in flowing binary suspensions of elastic capsules. *Phys. Rev. E* 84:066316.
18. Zhao, H., and E. Shaqfeh, 2011. Shear-induced platelet margination in a microchannel. *Phys. Rev. E* 83:061924.
19. Zhao, H., E. S. G. Shaqfeh, and V. Narsimhan, 2012. Shear-induced particle migration and margination in a cellular suspension. *Phys. Fluids* 24:011902.
20. Kumar, A., R. G. Henríquez-Rivera, and M. D. Graham, 2013. Flow-induced segregation in confined multicomponent suspensions: effects of particle size and rigidity. *J Fluid Mech* 738:423–462.
21. Wang, G., W. Mao, R. Byler, K. Patel, C. Henegar, A. Alexeev, and T. Sulchek, 2013. Stiffness Dependent Separation of Cells in a Microfluidic Device. *PLoS ONE* 8:e75901–10.
22. Fedosov, D. A., and G. Gompper, 2014. White blood cell margination in microcirculation. *Soft Matter* 10:2961–2970.
23. Müller, K., D. A. Fedosov, and G. Gompper, 2014. Margination of micro- and nano-particles in blood flow and its effect on drug delivery. *Sci. Rep.* 4:1–8.
24. Reasor, D. A., M. Mehrabadi, D. N. Ku, and C. K. Aidun, 2012. Determination of Critical Parameters in Platelet Margination. *Ann. Biomed. Eng.* 41:238–249.
25. Vahidkhah, K., S. L. Diamond, and P. Bagchi, 2014. Platelet Dynamics in Three-Dimensional Simulation of Whole Blood. *Biophys J* 106:2529–2540.
26. Vahidkhah, K., and P. Bagchi, 2015. Microparticle shape effects on margination, near-wall dynamics and adhesion in a three-dimensional simulation of red blood cell suspension. *Soft Matter* 11:2097–2109.
27. Munn, L. L., R. J. Melder, and R. K. Jain, 1996. Role of erythrocytes in leukocyte-endothelial interactions: mathematical model and experimental validation. *Biophys J* 71:466–478.
28. Decuzzi, P., S. Lee, B. Bhushan, and M. Ferrari, 2005. A Theoretical Model for the Margination of Particles within Blood Vessels. *Ann. Biomed. Eng.* 33:179–190.
29. Hund, S. J., and J. F. Antaki, 2009. An extended convection diffusion model for red blood cell-enhanced transport of thrombocytes and leukocytes. *Phys. Med. Biol.* 54:6415–6435.
30. Tokarev, A. A., A. A. Butylin, E. A. Ermakova, E. E. Shnol, G. P. Panasenko, and F. I. Ataulakhanov, 2011. Finite Platelet Size Could Be Responsible for Platelet Margination Effect. *Biophys J* 101:1835–1843.
31. Tokarev, A. A., A. A. Butylin, and F. I. Ataulakhanov, 2011. Platelet Adhesion from Shear Blood Flow Is Controlled by Near-Wall Rebounding Collisions with Erythrocytes. *Biophys J* 100:799–808.
32. Kumar, A., and M. Graham, 2012. Mechanism of Margination in Confined Flows of Blood and Other Multicomponent Suspensions. *Phys. Rev. Lett.* 109:108102.
33. Henríquez-Rivera, R. G., K. Sinha, and M. D. Graham, 2015. Margination Regimes and Drainage Transition in Confined Multicomponent Suspensions. *Phys. Rev. Lett.* 114:188101–5.
34. Fitzgibbon, S., A. P. Spann, Q. M. Qi, and E. S. G. Shaqfeh, 2015. In Vitro Measurement of Particle Margination in the Microchannel Flow: Effect of Varying Hematocrit. *Biophys J* 108:2601–2608.
35. Hou, H. W., A. A. S. Bhagat, A. G. Lin Chong, P. Mao, K. S. Wei Tan, J. Han, and C. T. Lim, 2010. Deformability based cell margination—A simple microfluidic design for malaria-infected erythrocyte separation. *Lab Chip* 10:2605.
36. Limbach, H. J., A. Arnold, B. A. Mann, and C. Holm, 2006.

- ESPResSo—an extensible simulation package for research on soft matter systems. *Comput. Phys. Commun.* 174:704–727.
37. Roehm, D., and A. Arnold, 2012. Lattice Boltzmann simulations on GPUs with ESPResSo. *Eur. Phys. J. Spec. Top.* 210:89–100.
 38. Arnold, A., O. Lenz, S. Kesselheim, R. Weeber, F. Fahrenberger, D. Roehm, P. Kosovan, and C. Holm, 2013. ESPResSo 3.1: Molecular Dynamics Software for Coarse-Grained Models, volume 89 of *Lecture Notes in Computational Science and Engineering*. Springer Berlin Heidelberg, Berlin, Heidelberg.
 39. Succi, S., 2001. *The Lattice Boltzmann equation for fluid dynamics and beyond*. Clarendon Press.
 40. Dünweg, B., and A. J. C. Ladd, 2009. Lattice Boltzmann simulations of soft matter systems. *Adv Polym Sci* 221:89–166.
 41. Aidun, C. K., and J. R. Clausen, 2010. Lattice-Boltzmann Method for Complex Flows. *Annu. Rev. Fluid Mech.* 42:439–472.
 42. Peskin, C. S., 2003. The immersed boundary method. *ANU* 11:479–517.
 43. Mittal, R., and G. Iaccarino, 2005. IMMERSED BOUNDARY METHODS. *Annu. Rev. Fluid Mech.* 37:239–261.
 44. Barthès-Biesel, D., 2011. Modeling the motion of capsules in flow. *Curr. Opin. Coll. Int. Sci.* 16:3–12.
 45. Freund, J. B., 2013. The flow of red blood cells through a narrow spleen-like slit. *Phys. Fluids* 25:110807.
 46. Farutin, A., T. Biben, and C. Misbah, 2014. 3D numerical simulations of vesicle and inextensible capsule dynamics. *J. Comput. Phys.* 275:539–568.
 47. Krüger, T., B. Kaoui, and J. Harting, 2014. Interplay of inertia and deformability on rheological properties of a suspension of capsules. *J Fluid Mech* 751:725–745.
 48. Krüger, T., F. Varnik, and D. Raabe, 2011. Efficient and accurate simulations of deformable particles immersed in a fluid using a combined immersed boundary lattice Boltzmann finite element method. *Computers and Mathematics with Applications* 61:3485–3505.
 49. Krüger, T., 2011. Computer simulation study of collective phenomena in dense suspensions of red blood cells under shear. Ph.D. thesis, Universität Bochum.
 50. Feng, Z.-G., and E. E. Michaelides, 2004. The immersed boundary-lattice Boltzmann method for solving fluid–particles interaction problems. *J. Comput. Phys.* 195:602–628.
 51. Freund, J. B., and M. M. ORESCANIN, 2011. Cellular flow in a small blood vessel. *J Fluid Mech* 671:466–490.
 52. Katanov, D., G. Gompper, and D. A. Fedosov, 2015. Microvascular blood flow resistance: Role of red blood cell migration and dispersion. *Microvasc. Res.* 99:57–66.